Optimization Design of High-Pressure Simulated Rotor

Zhongyu Yang[1,2,3(✉)], Jiali Chen[1,2,3], and Yinli Feng[1,3,4]

[1] Key Laboratory of Light Duty Gas Turbine, Institute of Engineering Thermophysics, Chinese Academy of Sciences, Beijing, China
yzyu889@163.com
[2] School of Aeronautics and Astronautics, University of Chinese Academy of Sciences, Beijing, China
[3] Innovation Academy for Light-Duty Gas Turbine, Chinese Academy of Science, Beijing, China
[4] School of Engineering Sciences, University of Chinese Academy of Sciences, Beijing, China

Abstract. Combined elastic support which include squirrel cage and squeeze film damper (SFD) are widely used in aero-engines, gas turbine, and steam turbine. Squirrel cage can vary the critical speed and strain energy distribution of the rotor system by changing the stiffness. SFD can effectively suppress rotor vibration and reduce transmitted forces. Given the inherently nonlinear behavior of SFD, a poorly designed damper has the potential to exacerbate rotor vibrations, posing a significant safety risk to engine operation. The influence of axial width of the SFD on dynamics behavior of the rotor-SFD system, such as critical speed, mode shape, vibration response has been developed in this paper. The Newton method was employed to optimize the critical speed and vibration response. The results of optimization reduced the 2nd critical speed by 24%, reduced the vibration amplitude of acceleration by 92%, and reduced the vibration amplitude of displacement by 88.3%. The contents and methods of this paper can provide guidance for the vibration optimization of rotor-squeeze film damper system.

Keywords: Width · Squirrel Cage · Critical Speed · Vibration · Newton method

1 Introduction

Combined elastic support which include squirrel cage and squeeze film damper (SFD) are widely used in rotating machines for its advantages of low cost, simple structure and outstanding vibration attenuation effect. However, it would cause complex motions of the rotor system under specific operating conditions.

The dynamic characteristics of combined elastic support have been extensively investigated by both theoretical and experimental approaches. Han et al. [1] established a finite element model of a rotor-squirrel cage-SFD system, and analyzed the effect of bearing bias on the squirrel cage. Luo et al. [2] established a finite element model considering the coupling effect between composite bearings and rotors, analyzed the nonlinear contact and oil film forces of composite bearings, and derived the high-dimensional partial

differential equations with local nonlinearity. Ma et al. [3] combined the finite element method with the free interface modal synthesis method to solve the dynamic equations of a dual-rotor-composite bearing system, analyzed the influence of unbalance on the nonlinear dynamic characteristics of the system and verified the results through experiments. Jaroslav Zapoměl et al. [4] investigated the influence of energy dissipation in the damping process of a rigid rotor-composite bearing system, and analyzed methods to minimize energy loss in rotor systems. Gao et al. [5] developed a finite element model for a flexible asymmetric rotor-SFD system and explored the influence of the coupling effect between combined elastic support and the rotor on the nonlinear characteristics of the rotor system. Chen et al. [6] derived the equations of motion for a rotor-SFD system considering inertial forces and static eccentricity, investigated the effects of structural parameters, unbalance, and stiffness of elastic support on the transient response of the rotor. Shao et al. [7] examined the impact of nonlinear oil film forces on the dynamic characteristics of a rotor system, and investigated the effects of structural parameters of the SFD on the vibration response. Luis San Andrés et al. [8] studied the impact of different end seals on the rotor dynamic characteristics, compared various methods for calculating damping coefficients and substantiated the result through experimental results. Kaihua Lu et al. [9] conducted experiments to revealed the influence of the viscosity of oil on the vibration characteristics of a rotor-combined bearing system, and analyzed the vibration reduction characteristics of the SFD.

The effect of axial width of SFD on damping characteristics of SFD has been analyzed in this paper based on the principles of rotor dynamics and fluid mechanics. Newton method was employed for the optimization of rotor dynamics to address the issue of excessive critical speed and vibration amplitude. Structural optimization is reasonable based on the calculation results of finite element method, which can provide a reference for the design of rotor.

2   Modeling of High-Pressure Simulated Rotor

Based on the situation of the experimental setup, the main design requirements for simulated rotor system are as follows:

(1) The maximum axial dimension of simulated rotor system is 1500 (mm) and the maximum radial dimension is 200 (mm).
(2) The maximum first two critical speeds of the rotor is 30000 (rpm).
(3) The maximum value of D/N of the rotor bearing is 2.5×10^6 (mmr/min).
(4) The bearing seat needs to provide enough space to arrange the lubrication oil path, ensuring the sealing and lubrication of the rotor system.

Based on the above requirements, the simulated rotor referenced the structure of a high-pressure rotor system in aircraft engines which mainly includes the disc, lubrication oil channel, locking nuts, gasket, and others. This simulated rotor adopted a 1-0-1 bearing configuration, the length of shaft in this model is 440 (mm), the maximum diameter is 50 (mm), and the weight is 17 (kg). The specific structure is shown in Fig. 1.

In this model, the diameter of journal of the SFD is 80 (mm), the outer diameter is 82 (mm), and the width is 15 (mm). The specific structure of the SFD is shown in Fig. 2.
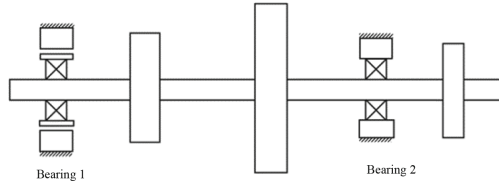
Fig. 1. Schematic diagram of the simulated rotor system structure
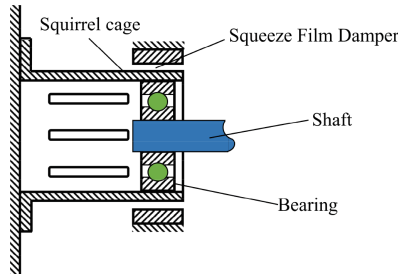

Fig. 2. Schematic diagram of the SFD structure

In this model, the number of bars in the squirrel cage is 8, the length is 30 (mm), the width is 4.1 (mm), the thickness is 2 (mm). The specific structure of the squirrel cage is shown in Fig. 3.
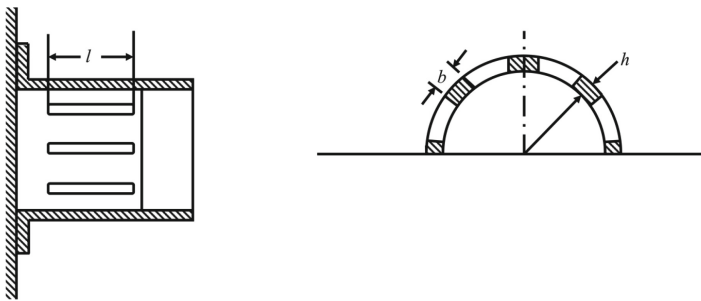

Fig. 3. Schematic diagram of the squirrel cage structure

A computational model for the damping characteristics has been established based on the theories of fluid mechanics and rotor dynamics. The results of the finite element method indicate that the rotor has superior overall rigidity and high strength. The strain energy distribution in this rotor system is reasonable, which ensures normal operation of the rotor. However, the 2nd critical speed exceeds 30000 (rpm), and the vibration amplitude of the rotor system exceeds the expected level, which severely affects the stability of the system during operation.

Regarding the aforementioned issue, an optimized design for the rotor system had been presented in this paper. Firstly, the influence of the squirrel cage structure on

stiffness have been determined, and the impact of the axial width of SFD on the stiffness and damping coefficient was investigated. Accordingly, the finite element method was employed to determine the stiffness and damping coefficient which meet the engineering requirements. Finally, the appropriate parameters of squirrel cage structure and the axial width of SFD were selected using the Newton method. The detailed explanation has been provided in Chapter 3.

3   Optimization of the Simulated Rotor System

This design optimization prioritizes varying the critical speed by changing the structure of the squirrel cage, and reducing the vibration amplitude of the rotor system by selecting an appropriate axial width of the SFD. The calculation model for the damping characteristics of SFD and the Newton method have been used to optimize the rotor system. This optimization method can serve as a reference for engineering practice.

3.1   Damping Characteristic Calculation Mode

For the rotor-SFD system, the damping properties of the oil film are crucial. The bearing 1 utilizes a combination elastic supporting structure consisting of SFD, squirrel cage, and rolling bearing, while bearing 2 adopts a rigid supporting structure with ball bearing. The schematic diagram of the SFD is shown in Fig. 4.
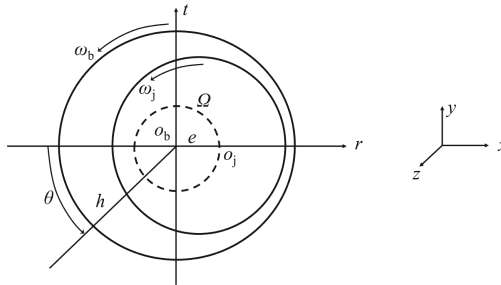

Fig. 4. Schematic diagram of the SFD

The basic equation for calculating the oil film force of the SFD is the generalized Reynolds equation for the hydrodynamic bearings [10]. The equation in Cartesian coordinates can be expressed as:

$$\frac{\partial}{\partial x}\left(\frac{\rho h^3}{\mu} \cdot \frac{\partial p}{\partial x}\right) + \frac{\partial}{\partial z}\left(\frac{\rho h^3}{\mu} \cdot \frac{\partial p}{\partial z}\right)$$
$$= 6\left(\omega_b + \omega_j - 2\Omega\right)\frac{\partial(\rho h)}{\partial \theta} + 12\frac{\partial(\rho h)}{\partial t} + 12\Omega h\frac{\partial \rho}{\partial \theta} \tag{3.1}$$

where, ρ is the density of the lubricant, h is the oil film thickness, μ is the viscosity of the lubricant, p is the oil film pressure, ω_b, ω_j are the angular velocities of the bearing and journal respectively, and Ω is the angular velocity of the journal orbiting.

The Reynolds equation for compressible flow in polar coordinates as follows:

$$\frac{\partial}{\partial \theta}\left(\frac{\rho h^3}{\mu}\cdot\frac{\partial p}{\partial \theta}\right) + R^2 \frac{\partial}{\partial z}\left(\frac{\rho h^3}{\mu}\cdot\frac{\partial p}{\partial z}\right)$$
$$= 6R^2\left(\omega_b + \omega_j - 2\Omega\right)\frac{\partial(\rho h)}{\partial \theta} + 12R^2\frac{\partial(\rho h)}{\partial t} + 12\Omega h\frac{\partial \rho}{\partial \theta} \quad (3.2)$$

where, R is the radius of the journal, e is the radial velocity.

When $\omega_b = \omega_j = 0$, $\rho = 0$, $\mu = 0$. The transient Reynolds equation for the SFD can be simplified to:

$$\frac{\partial}{\partial \theta}\left[(1 + \varepsilon\cos\theta)^3\frac{\partial p}{\partial \theta}\right] + R^2\frac{\partial}{\partial z}\left[(1 + \varepsilon\cos\theta)^3\frac{\partial p}{\partial z}\right]$$
$$= \frac{12\mu R^2}{c^2}(\varepsilon\Omega\sin\theta + \dot{\varepsilon}\cos\theta) \quad (3.3)$$

where, c is the average gap of the oil film, ε is the eccentricity of the SFD, and $\varepsilon = e/c$, $h = c + e\cos\theta$.

In the prototype SFD, there are no hermetic seals at both ends, and the pressure at either end is similar to the external pressure. Due to the squeezing effect, the pressure in the central region of the damper is considerably higher, while the circumferential pressure gradient is low, as in (3.4):

$$\frac{\partial p}{\partial z} >> \frac{\partial p}{\partial \theta} \quad (3.4)$$

Equation (3.3) can be simplified as:

$$\frac{\partial}{\partial z}\left[(1 + \varepsilon\cos\theta)^3\frac{\partial p}{\partial z}\right] = \frac{12\mu}{c^2}(\varepsilon\Omega\sin\theta + \dot{\varepsilon}\cos\theta) \quad (3.5)$$

The hypothesis of short bearing theory is available when $L/D < 0.25$. Taking the central section of the damper as the coordinate axis and using atmospheric pressure as the reference point, the boundary conditions at $z = -L/2$ are $p = p_1 = 0$, and at $z = L/2$ are $p = p_2 = 0$, as shown in Fig. 5. Integrating (3.5) twice with respect to z yields the pressure distribution of the oil film.

$$p(\theta, z) = -\frac{6\mu}{c^2(1 + \varepsilon\cos\theta)^3}(\varepsilon\Omega\sin\theta + \dot{\varepsilon}\cos\theta)(\frac{L^2}{4} - z^2) \quad (3.6)$$

where, L is the width of the SFD, D is the diameter of the SFD.

The radial and tangential forces on the journal caused by the pressure of the lubricant film in the damper can be calculated with the following formula:

$$\left\{\begin{array}{c} F_r \\ F_t \end{array}\right\} = \int_{-L/2}^{L/2}\int_{\theta_1}^{\theta_2} -p(\theta, z)\left\{\begin{array}{c} \cos\theta \\ \sin\theta \end{array}\right\}R d\theta dz \quad (3.7)$$
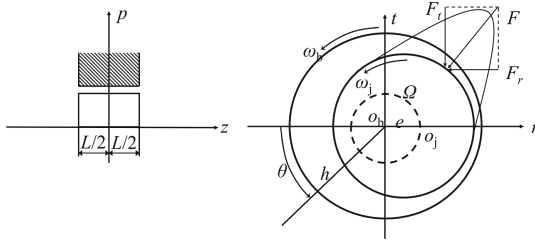
Fig. 5. Stress analysis diagram of SFD

Substituting (3.6) into (3.7), when the system is in the half-film state with $\theta_1 = \Pi$ and $\theta_2 = 2\Pi$, the radial and tangential forces on the journal can be determined as follows:

$$\begin{cases} F_r = \dfrac{\mu R L^3}{c^2} \cdot \left[\dfrac{2\Omega\varepsilon^2}{(1-\varepsilon^2)^2} + \dfrac{\pi\,\dot{\varepsilon}(1+2\varepsilon^2)}{(1-\varepsilon^2)^{5/2}} \right] \\[4mm] F_t = \dfrac{\mu R L^3}{c^2} \cdot \left[\dfrac{\pi\,\Omega\varepsilon}{(1-\varepsilon^2)^{3/2}} + \dfrac{2\varepsilon\,\dot{\varepsilon}}{(1-\varepsilon^2)^2} \right] + (p_1 + p_2)LR \end{cases} \tag{3.8}$$

When the system is in the full-film state with $\theta_1 = 0$ and $\theta_2 = 2\Pi$, the radial and tangential forces on the journal can be determined as follows:

$$\begin{cases} F_r = \dfrac{\mu R L^3}{c^2} \cdot \dfrac{\pi\,\dot{\varepsilon}(1+2\varepsilon^2)}{(1-\varepsilon^2)^{5/2}} \\[4mm] F_t = \dfrac{\mu R L^3}{c^2} \cdot \dfrac{\pi\,\Omega\varepsilon}{(1-\varepsilon^2)^{3/2}} \end{cases} \tag{3.9}$$

The stiffness coefficient K and damping coefficient C of the SFD are:

$$\begin{cases} K = -\dfrac{F_r}{e} \\[4mm] C = -\dfrac{F_t}{e\Omega} \end{cases} \tag{3.10}$$

The negative sign represents wherein the distribution of radial force and tangential force is opposite to the direction of the eccentricity and precession speed.

3.2 Calculation Model for Squirrel Cage

The advantages of using a squirrel cage are that it can control the critical speed and the distribution of strain energy of the rotor system by changing the stiffness of the squirrel cage. The cross-section of the squirrel cage closes to rectangular, and the radial stiffness and axial stiffness of the bars are not equal. Therefore, under the action of the radial force F transmitted by the bearing, the load distributed to each bar is different. The boundary conditions at both ends of the cage bars are depicted in Fig. 6. It is assumed that one end is fixed and the other end is constrained to undergo only radial displacement without any rotational degrees of freedom.
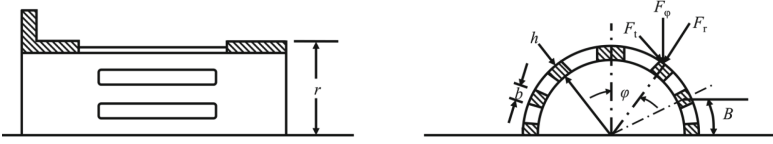
Fig. 6. The force model of squirrel cage

When one end of the cage bar is subjected to a force F_φ resulting from the F, it is equivalent to a free end with an additional bending moment, the value of which is:

$$M_\varphi = \frac{F_\varphi l}{2} \tag{3.11}$$

where, l is the length of the cage bar.

The displacement at the end of the cage bar can be calculated as follows:

$$Y = \frac{F_\varphi l^3}{12EJ} \tag{3.12}$$

Since the cross-section of the cage bar is rectangular and the direction of the force is not aligned with the principal axis of the cross-section, the displacement should be calculated along the principal axis. The radial and circumferential displacements of the cage bar can be calculated as follows:

$$Y_r = Y \cos \varphi, \, F_r = F_\varphi \cos \varphi$$
$$Y_t = Y \sin \varphi, \, F_t = F_\varphi \sin \varphi \tag{3.13}$$

where, Y_r is the radial displacement, F_r is the radial load, Y_θ is the circumferential displacement, and F_θ is the circumferential load.

The moments of inertia about the radial and circumferential axes are given respectively by:

$$J_r = \frac{bh^3}{12}$$
$$J_t = \frac{hb^3}{12} \tag{3.14}$$

where, J_r is the moment of inertia of the radial axes, J_t is the moment of inertia of the circumferential axes.

The total displacement of the cage bar in the direction of force is:

$$Y = Y_t \sin \varphi + Y_r \cos \varphi = \frac{F_\varphi l^3}{E} [\frac{\cos^2 \varphi}{h^3 b} + \frac{\sin^2 \varphi}{hb^3}] \tag{3.15}$$

If the force acting on the differential segment of the cage bar is df, then:

$$df = F_\varphi \frac{rd\varphi}{B} \tag{3.16}$$

where, r is the radius, and B is the arc length between two cage bars.

Substituting (3.15) into (3.16):

$$df = E\frac{b^3 h^3}{l^3 B} rY \frac{d\varphi}{b^2 \cos^2 \varphi + h^2 \sin^2 \varphi} \tag{3.17}$$

$$\int_0^\pi \frac{d\varphi}{b2 \cos 2\varphi + h2 \sin 2\varphi} = \frac{2}{bh}(\pi + i2\pi) \tag{3.18}$$

where, i is 0 and a positive integer.

When $i = 0$.

$$\int_0^\pi \frac{d\varphi}{b2 \cos 2\varphi + h2 \sin 2\varphi} = \frac{2\pi}{bh} \tag{3.19}$$

The total force F acting on the entire squirrel cage is:

$$F = \int_0^{2\pi} df = \frac{2\pi r b^2 h^2 YE}{l^3 B} \tag{3.20}$$

The stiffness coefficient of the entire squirrel cage is:

$$k = \frac{F}{Y} = \frac{2\pi r b^2 h^2 E}{l^3 b} \tag{3.21}$$

3.3 Newton Method

The Newton method is characterized by its rapid convergence and simple implementation, which makes it widely utilized for solving nonlinear optimization problems. The Hessian matrix of a multivariate function takes on the following form:

$$H_f = \begin{bmatrix} \dfrac{\partial^2 f}{\partial x_1^2} & \dfrac{\partial^2 f}{\partial x_1 \partial x_2} \\ \dfrac{\partial^2 f}{\partial x_1 \partial x_2} & \dfrac{\partial^2 f}{\partial x_2^2} \end{bmatrix} \tag{3.22}$$

The gradient of the function is as follows:

$$\nabla f(x_1, x_2) = (\frac{\partial f}{\partial x_1}, \frac{\partial f}{\partial x_2})^T \tag{3.23}$$

Let the independent variable be $x = (x_1, x_2)^T$ then the iterative formula can be expressed as:

$$x^{k+1} = x^k - H_f^{-1}(x)\nabla f(x) \tag{3.24}$$

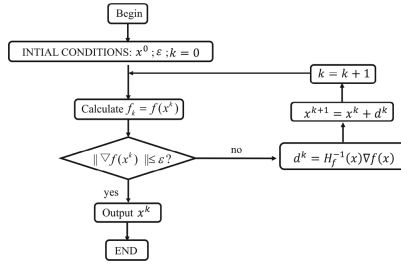The computation process of the Newton method is shown in Fig. 7.

Fig. 7. The computation process of the Newton method

3.4 Dynamic Analysis of the Original Rotor System

The stiffness of bearing 1 of the original rotor system is 5×10^6 (N/m), the stiffness of bearing 2 is 1×10^8 (N/m), the journal diameter of SFD is 80 (mm), the width of SFD is 15 (mm), the eccentricity of SFD is 0.1, and the clearance of SFD is 0.2 (mm). The critical speeds of the rotor's first three orders were calculated using rotor dynamic analysis software, as shown in Table 1. The transient response of the bearing 1 during the acceleration process is shown in Fig. 8. And Fig. 9. As can be seen, The 2nd critical speed is higher than the design requirement, and the vibration amplitude of the rotor system is relatively large during the acceleration process, which seriously endangers the stable operation of the rotor system.

Table 1. The critical speeds of the original system

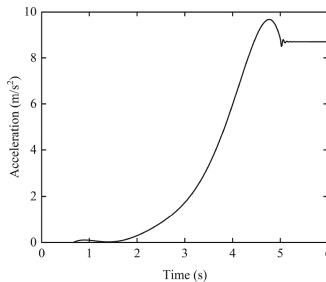|	Critical Speed (rpm)
1st order	20567
2nd order	32849
3rd order	103155

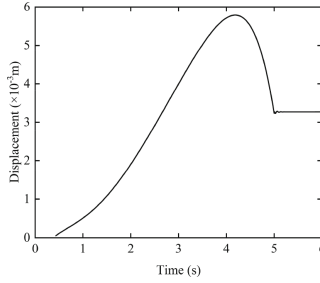**Fig. 8.** Transient response of acceleration of the bearing 1 in the original rotor system

Fig. 9. Transient response of displacement of the bearing 1 in the original rotor system

3.5 The Impact of Axial Width of SFD on Damping Characteristics

The impact of axial width of SFD on the damping characteristics of the SFD is shown in Fig. 10. And Fig. 11. An increase in axial width of SFD leads to an increase in the effective area of oil film extrusion, and resulting in an increasing trend of oil film damping and a decrease in oil film stiffness. The damping coefficient also exhibits an increase in nonlinearity while the stiffness coefficient consistently displays nonlinear characteristics.
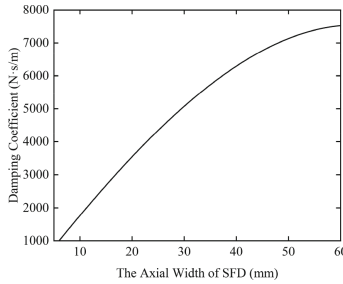

Fig. 10. The variation law of the damping coefficient with the axial width of SFD
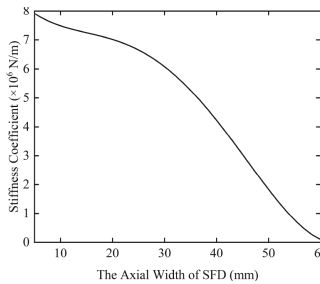

Fig. 11. The variation law of the stiffness coefficient with the axial width of SFD

3.6 Optimization of the Simulated Rotor System

According to the analysis above, the original rotor system can be concluded to have issues of high 2nd critical speed and excessive vibration amplitude. This will seriously endanger the stable operation of the rotor system during acceleration. Therefore, measures need to be taken to reduce the 2nd critical speed, decrease the vibration amplitude, and improve stability and reliability.

Firstly, regarding the issue of higher 2nd critical speed, as analyzed above, it is known that the stiffness of the squirrel cage has a significant impact on the critical speed of the rotor system. The initial parameters of the original squirrel cage were chosen as the starting point for the optimization algorithm, with the stiffness of squirrel cage being 4.6×10^6 (N/m). The Newton method was used to screen the data along the reverse gradient direction. Finally, it was determined, when the stiffness of squirrel cage was 5.7×10^5 (N/m), the 2nd critical speed met the design requirements. At this point, the number of bars in the squirrel cage is 6, the length is 40 (mm), the width is 3 (mm), the thickness is 1.8 (mm). The optimized rotor system has the first three critical speeds as shown in Table 2, with the 1st critical speed at 14651 (rpm) and the 2nd critical speed at 25263 (rpm), which meet the design requirements (2). The optimized squirrel cage was subjected to strength verification, and the results showed that it has good mechanical properties, which can ensure the normal operation of the rotor system.

Table 2. The critical speeds of the optimized system

	Critical Speed (rpm)
1st order	14651
2nd order	25263
3rd order	57979

To address the problem of excessive vibration amplitude in the rotor system, this paper, considering the design constraints of the rotor system, such as critical speed and the DN value of the bearings, proposes the solution of increasing the damping effect of SFD by changing the size of axial width of SFD. The initial parameters of the original rotor system were chosen as the starting point for the optimization algorithm, with the axial width of the SFD is 15 (mm). The Newton method was used to screen the data along the reverse gradient direction. Finally, it was determined, when the axial width of the SFD was increased to 40 (mm), the vibration of the rotor system met the design requirements. The transient response of the bearing 1 during the acceleration process were shown in Fig. 12. And Fig. 13. The optimized rotor was subjected to strength verification, and the results showed that the overall rigidity of the rotor is relatively high, the strain energy distribution in the rotor system is reasonable, and meets the design requirements, which can ensure the normal operation of the rotor.
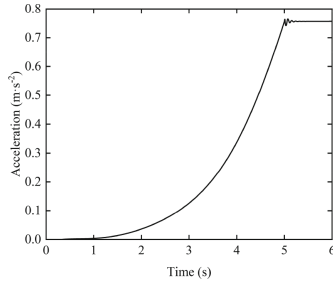
Fig. 12. Transient response of acceleration of the bearing 1 in the optimized rotor system
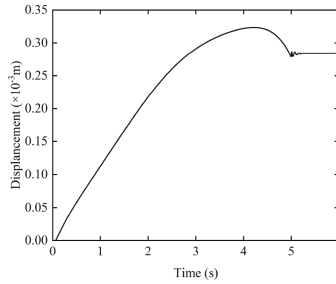

Fig. 13. Transient response of displacement of the bearing 1 in the optimized rotor system

4   Conclusion

Based on the finite element method, this paper analyzed the problems in the finite element model of the high-pressure simulated rotor and proposed optimization measures to address these shortcomings. The following conclusions were drawn:

- The axial width of the SFD directly affects the stiffness and damping of the squeeze film, and changing the axial width of the SFD within a certain range can effectively reduce the vibration amplitude of the rotor system.
- To reduce the 2nd critical speed, this paper used Newton method to obtain the optimal solution for the stiffness of the squirrel cage, and adjusting the structural parameters of the squirrel cage.
- To reduce the vibration amplitude of the rotor system, this paper used Newton method to obtain the optimal solution for the axial width of the SFD, which effectively reduced the vibration amplitude and improved the stability and reliability of the rotor system.
- Through the rotor dynamic analysis of the optimized simulated rotor, the results showed the optimized rotor system possesses favorable rotor dynamic characteristics and can meet all design requirements, which can provide support for subsequent research.

References

1. Han, Q., Chen, Y., Zhang, H., et al.: Vibrations of rigid rotor systems with misalignment on squirrel cage supports. J. Vibroeng. **18**(7), 4329–4339 (2016)
2. Luo, Z., Wang, J., Tang, R., et al.: Research on vibration performance of the nonlinear combined support-flexible rotor system. Nonlinear Dyn. **98**, 113–128 (2019)
3. Xinxing, M.A., Hui, M.A., Haiqin, Q.I.N., et al.: Nonlinear vibration response characteristics of a dual-rotor-bearing system with squeeze film damper. Chin. J. Aeronaut. **34**(10), 128–147 (2021)
4. Zapoměl, J., Ferfecki, P., Kozánek, J.: Application of the controllable magnetorheological squeeze film dampers for minimizing energy losses and driving moment of rotating machines. In: Cavalca, K.L., Weber, H.I. (eds.) 10th International Conference on Rotor Dynamics, vol. 60, pp. 132–143. Mechanisms and Machine Science (2018)
5. Tian, G.A.O., Shuqian, C.A.O., Yongtao, S.U.N.: Nonlinear dynamic behavior of a flexible asymmetric aero-engine rotor system in maneuvering flight. Chin. J. Aeronaut. **33**(10), 2633–2648 (2020)
6. Chen, X., Gan, X., Ren, G.: Dynamic modeling and nonlinear analysis of a rotor system supported by squeeze film damper with variable static eccentricity under aircraft turning maneuver. J. Sound Vib. **485**, 1879–1928 (2020)
7. Shao, J., Jigang, W., Cheng, Y.: Nonlinear dynamic characteristics of a power-turbine rotor system with branching structure. Int. J. Non-Linear Mech. **148**, 21–37 (2022)
8. Andrés, L.S., Koo, B., Jeung, S.-H.: Experimental force coefficients for two sealed ends squeeze film dampers (Piston Rings and O-Rings): an assessment of their similarities and differences. J. Eng. Gas Turb. Power-Trans. ASME **141**(2), 1–13 (2019)
9. Kaihua, L., He, L., Yan, W.: Experimental study of Iersfds for vibration reduction of gear transmissions. J. Vibroeng. **21**(2), 409–419 (2019)
10. Jialiu, G.: Dynamic Characteristics of Rotors with Squeeze Film Dampers, 1st edn. National Defence Industry Press, Beijing (1985)